

# Ordering of carbon in highly supersaturated $\alpha$ -Fe

Osamu Waseda<sup>1</sup>, Julien Morthomas<sup>1</sup>, Fabienne Ribeiro<sup>2</sup> ,  
Patrice Chantrenne<sup>1</sup>, Chad W Sinclair<sup>3</sup> and Michel Perez<sup>1</sup> 

<sup>1</sup> Université de Lyon, INSA Lyon, MATEIS, UMR CNRS 5510, Villeurbanne, France

<sup>2</sup> IRS[N], PSN, SEMIA, LPTM, Saint-Paul-Lez-Durance, France

<sup>3</sup> The Department of Materials Engineering, The University of British Columbia, 309-6350 Stores Road, Vancouver, British Columbia, V6T 1Z4, Canada

E-mail: [Michel.Perez@insa-lyon.fr](mailto:Michel.Perez@insa-lyon.fr)

Received 13 July 2018, revised 28 August 2018

Accepted for publication 7 November 2018

Published 12 December 2018



CrossMark

## Abstract

Metropolis Monte Carlo is used to investigate the Zener ordering as the carbon content of body centered cubic iron is increased. Thanks to a fast simulation algorithm, the equilibrium state for a wide range of temperature and carbon content are investigated. These results are compared to a thermodynamical mean-field model that accounts for long range elastic interaction and configurational entropy. At carbon levels of above 2 at.%, it is found that the mean-field model overestimates the order–disorder transition temperature. This is due to local repulsive C–C interactions not accounted for in the mean-field model. Forbidding some strongly repulsive configurations leads to a better agreement between the mean-field model and Metropolis Monte Carlo simulations. At high concentration carbon atoms in solid solution exhibits local configurations typical of the  $\text{Fe}_{16}\text{C}_2$  carbide.

Keywords: ordering, Monte Carlo, molecular dynamics, Fe–C

(Some figures may appear in colour only in the online journal)

## 1. Introduction

The richness of the simple binary Fe–C system continues to provide new opportunities for tailoring the physical, functional and mechanical properties of ferrous alloys. While the equilibrium phase diagram, pioneered by Roberts-Austen in 1897 [1], is well established, our understanding of the large number of metastable phases not appearing on the phase diagram is far from well understood. Metastable iron carbides find use in applications ranging from magnetic recording media [2] to catalysts [3, 4]. The single largest use of metastable Fe–C

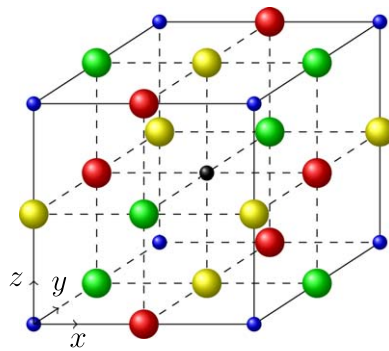


**Figure 1.** Three different site types that one C atom can assume in different colors. In the following, the site types *x*, *y* and *z* refer to interstitial sites represented by yellow, green and red spheres, respectively. Fe atoms are represented in small blue spheres.

phases, however, is in structural steel components. Due to its low solubility limit in Fe, C would form C-rich phases in relatively limited amount. Therefore, new routes have to be found to reach high level of supersaturation that finds application to strengthen the material [5].

There are a variety of examples of processes which have been argued to lead to high levels of carbon supersaturation in ferrite. Deformation processing by wire drawing, ball milling, or other severe plastic deformation processes is well known to lead to the dissolution of carbides and the formation of supersaturated ferrite [6–8]. The ability to create colossal carbon supersaturation in ferrite by means of vapour deposition has been revisited [9–12]. Martensite ( $\alpha'$ -Fe), itself a metastable supersaturated form of ferrite, can contain a large amount of C atoms in solid solution. While a large percentage of C atoms segregate to defects (dislocations, lath boundaries) during autotempering [13–16], if not during (auto) tempering some may remain locally in solid solution due to high levels of residual stresses. Even bainitic ferrite has been recently claimed to contain abnormally high levels of C [17, 18].

Whatever the mechanism used to obtain these supersaturated states, the structure remains body centered cubic (BCC) or body centered tetragonal (BCT) iron. In BCC iron, C atoms can occupy three types of octahedral interstitial sites (cf figure 1). If C atoms occupy one interstitial site type (ordered phase), tetragonal distortion is observed (e.g. martensite). If C atoms occupy all site types randomly (disordered phase), the matrix remains cubic.

The deformation of the lattice due to this tetragonality has been experimentally measured via x-ray diffraction (see the compilation of literature data of Xiao *et al* [19]). Some investigations showed that tetragonality disappears at lower C concentrations [19], assuming an ‘order–disorder’-like transition. The temperature and pressure dependence of such transition has not yet been fully understood since segregation of C to defects could also explain the loss of tetragonality [11, 12, 20–25].

The mechanism of the order–disorder transition of supersaturated ferrite was first described by Zener [26]. In his theory, the C ordering is described via elastic strain interactions between carbon atoms. Thus leads to the conclusion that above a critical carbon concentration and below a critical temperature, all carbon atoms should reside in one type of octahedral site. This model being mean field, does not account for neighbour carbon atom interactions something that may expect to be important for finite carbon concentrations.

A more rigorous treatment was developed by Khachaturian [27], as part of the so-called microscopic elasticity theory (MET). In the MET treatment of interstitial ordering driven by

elasticity, atomistic information is encoded in the form of simplified C–C chemical interactions, depending only on the distance between C atoms. Udyansky *et al* [28] have re-evaluated the prediction of the order–disorder transition in supersaturated ferrite using MET parameterized via a semi-empirical EAM potential for the Fe–C system. Recently, Maugis *et al* [29] clarified Zener’s original calculation. They demonstrated that elastic mean field theory leads to a thermodynamic hysteresis in order–disorder temperature.

Using the empirical Calphad method, Naraghi *et al* [30] proposed a rather complete Fe–C phase diagram including some metastable carbides and accounting for the order–disorder transition.

Chirkov *et al* [31] predicted the order–disorder transition performing molecular statics (MS) and molecular dynamics (MD) simulations combined with mean field Zener thermodynamical calculation, using the interatomic potential developed by Lau *et al* [32]. In this study, the MET is used, in which the potential energy variation was calculated by taking the energy difference between an ordered and a disordered state, while these states were minimised via MS. However, to create the ordered and disordered states, the C atoms were inserted randomly into the Fe-matrix, meaning the C atoms were not distributed in a physically meaningful way.

The importance of short ranged C–C interaction missing in the above methods was highlighted in the work of Ruban [33]. Ruban demonstrated the importance of bringing the mean field description further to include direct interactions of individual C atoms via DFT calculations. MD simulations [34] using the Raulot–Becquart EAM interatomic potential (RB-potential) [35], confirmed the stability of the ordered phase as a function of C content and temperature. However temperature was limited to 800 K and higher, due to the slow diffusion of C relative to characteristic MD computation time.

In this paper we investigate the thermal stability of supersaturated BCC iron via Metropolis Monte Carlo (MeMC). We focus here on relatively high carbon contents, for which C–C interaction play a major role. In addition, the Zener thermodynamic mean-field model will be revisited and presented in a rather simple form. We will confirm that such mean field models cannot account for local ordering that may drastically change the thermal stability of ordered and disordered phases. The MeMC approach makes it possible to scan a wider range of temperatures and carbon compositions than our previous work [34]. Note that in this range of temperature and composition, carbides are supposed to be present at equilibrium. However, since our goal is to better understand ordering in  $\alpha$ -iron, precipitates are not considered in this paper.

## 2. Simulation methodology

In this section, the potential, the simulation box and the methods (MeMC and MD) used in this paper will be presented. MeMC will be used to determine the order–disorder transition temperatures, whereas MD will be used only for generating additional ordered and disordered configurations at 8 and 9 at. %.

### 2.1. Choice of interatomic potential

The energetics of the studied system is supplied by the RB empirical Embedded Atom Method (EAM) Fe–C potential [35, 36]. This potential predicts the experimentally observed trend for tetragonality of ferrite as a function of carbon and an accurate description of the diffusion coefficient of carbon [37]. It has also been tested for more concentrated systems up

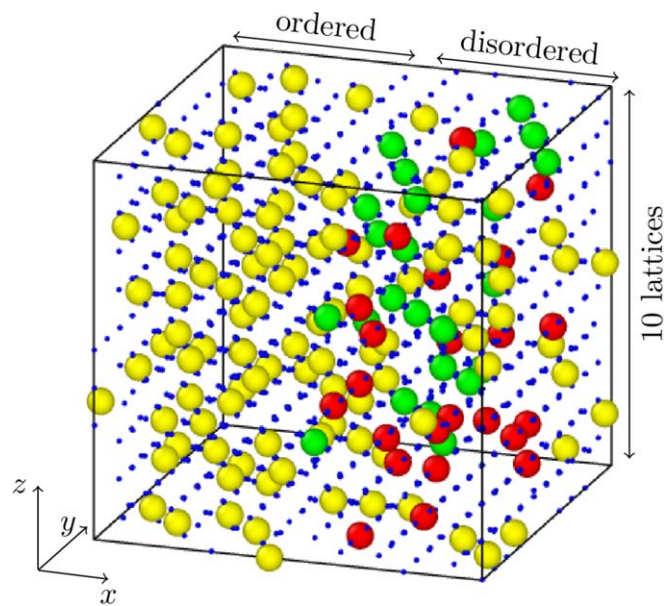


**Figure 2.** Initial configuration for partially ordered box. Small blue spheres represent Fe atoms. C atoms are colored according to their tetragonality induced (x, y and z are each yellow, green and red).

to 11 at.% [34] and for non-homogeneous systems for which carbon is strongly segregated around dislocations [38–40].

## 2.2. Simulation boxes

Simulation boxes containing 2000 Fe atoms ( $10 \times 10 \times 10$  lattices) arranged on a bcc lattice are generated with C concentrations ranging from 1 to 11 at.%. Three different kinds of simulation boxes are generated: fully ordered, fully disordered and half-ordered/half-disordered.

**2.2.1. Ordered simulation boxes.** Fully ordered simulation boxes are generated, for which C atoms sit exclusively on z-sites. In order to avoid high energy configurations of neighboring C atoms, these boxes are relaxed with 100 000 MeMC steps (C atoms exchange and local relaxation, see section 2.3) at 600 K, for which C atoms are forced to remain in the same site type during the Metropolis exchanges.

**2.2.2. Disordered simulation boxes.** Fully disordered simulation boxes are also generated, for which C atoms sit randomly x, y or z-sites. These boxes are then relaxed with 100 000 MeMC steps at 600 K, for which C atoms are forced to remain in the same site type during the Metropolis exchanges.

**2.2.3. Half-ordered / half-disordered simulation boxes.** Finally, to accelerate the convergence of simulations, initial simulation boxes can also be composed of two zones: the left half of the simulation box contains C atoms located randomly on z-sites only, whereas the other half of the simulation box contains C atoms located randomly on x, y and z-sites (see figure 2). The

energy of this system is then minimized using a conjugate gradient scheme (CG), including box size relaxation to minimise the stress (convergence is fulfilled when forces are lower than  $10^{-8}$  eV/Å and stresses are lower than 1 MPa). 10 000 initial steps of MeMC are performed, for which C atoms are forced (i) to remain in the same site type, and, (ii) to remain in the same half of the simulation box during MeMC exchanges. This initial MeMC simulation is performed at the same temperature as the subsequent MeMC or MD simulation.

For all generated systems, two C atoms are not allowed to sit within a distance of one lattice parameter, which would lead to unphysical high energy configurations due to C–C repulsive interactions.

### 2.3. Metropolis Monte Carlo

Classical atomistic MeMC simulations do not naturally account for local elastic distortions. However, to study the order–disorder transition governed by elastic interaction and local atomic configurations, it is vital that both global elastic and local interactions are accounted for. To realize this, a coupled MS-MeMC approach is used here (see detailed algorithm in [39, 40]). MeMC is particularly adapted to study the ordering of C atoms in ferrite since the number of configurations is high but tractable in a reasonable computing time.

At each MeMC step, one carbon atom is randomly selected and displaced to a randomly selected, unoccupied octahedral site, which does not have another C atom within a distance of one lattice parameter. Relaxation (at constant box volume) is then performed by MS with the CG method. The energies (i) of the system before moving the carbon atom and, (ii) after its displacement and the subsequent relaxation of the system, are then calculated. The displacement of the carbon atom is directly accepted if the internal energy change of the system  $\Delta U$  is negative. Otherwise it is accepted with a probability  $P$  defined by

$$P = \exp\left(-\frac{\Delta U}{k_B T}\right) \quad (1)$$

where  $k_B$  is the Boltzmann constant and  $T$  is the temperature. To avoid the build up of macroscopic stresses, that could couple to the elastic strain fields of individual carbon atoms, the box is relaxed via the CG method including box size relaxation every each 1000 MeMC steps. The macroscopic stresses on the box are thus maintained below 100 MPa (validating thus the minimisation protocol where the pressure contribution to energy is small compared to the enthalpy change:  $d(pV) \ll dU$ ).

The MeMC simulations are performed for temperatures ranging from 100 K to 1400 K (every 100 K) and the C content ranging from 1 at.% to 11 at.% (every 1 at.%).

### 2.4. Molecular dynamics

MD simulations were launched for C contents of 8 at.% and 9 at.%. To obtain ordered and disordered states, simulations were performed under NPT conditions during 100 ns ( $2 \times 10^8$  timesteps) at 900 K and 1400 K, respectively, and zero pressure. In contrast to [34], MD is used here only to provide ordered and disordered configurations. It has been checked that MD simulations performed at 900 K lead to ordered configurations with  $Z_{8\%} = 0.85$  and  $Z_{9\%} = 0.94$ , whereas simulations performed at 1400 K lead to disordered configurations with  $Z_{8\%} = 0.01$  and  $Z_{9\%} = 0.01$ .

### 3. Thermodynamic model

In this section, the Gibbs energy  $G = U + pV - TS$  of FeC systems will be calculated. The pressure  $p$  will be assumed to be zero and the entropy  $S$  will be estimated from the number of configurations.

This energy depends on temperature  $T$ , carbon concentration defined as  $x_C = n_C/(n_C + n_{Fe})$  (or carbon site-fraction  $X = n_C/(3n_{Fe})$ ) and order parameter  $Z$ , where  $n_C$  and  $n_{Fe}$  are the numbers of C and Fe atoms. We define  $n_C^x$ ,  $n_C^y$ ,  $n_C^z$  as the numbers of C atoms occupying  $x$ ,  $y$  and  $z$  site types, respectively (cf. figure 1). In this section we assume that ordering occurs only on  $z$ -sites such that fully disordered case corresponds to  $n_C^x = n_C^y = n_C^z = n_C/3$  and fully ordered case corresponds to  $n_C^x = n_C^y = 0$  and  $n_C^z = n_C$ . The order parameter  $Z$  is then defined as [41]

$$Z = \frac{3n_C^z/n_C - 1}{2} = \frac{n_C^z - n_C^x}{n_C}. \quad (2)$$

Equilibrium  $Z$  value is obtained by calculating the minimum of the Gibbs energy. The internal energy is assumed to depend on the carbon configuration exclusively via elastic interactions. The Gibbs energy is given by (detailed calculation can be found in the [appendix](#)):

$$G(X, Z, T) - G(X, 0, T) = U(X, Z, T) - U(X, 0, T) - T[S(X, Z, T) - S(X, 0, T)]. \quad (3)$$

The enthalpy change is assumed to depend only on elastic energy via elasticity theory. It is defined as (see the [appendix](#)):

$$U(X, Z, T) - U(X, 0, T) = 3n_{Fe}\lambda_0 X^2 Z^2 \quad (4)$$

where  $\lambda_0$  is the interaction parameter, which is defined as:

$$\lambda_0 = \frac{(1 + \nu)(\lambda' - \lambda)^2}{v_{at}E} \quad (5)$$

where  $\nu$  is the apparent Poisson coefficient ( $\nu = -S_{12}/S_{11}$ , where  $S_{ij}$  are the component of the compliance tensor),  $E$  is the apparent Young's modulus ( $E = 1/S_{11}$ ),  $\lambda$  and  $\lambda'$  are the diagonal components of the dipole tensor (defined in [42]) and  $v_{at}$  is the atomic volume. The  $\lambda_0$  parameter is calculated from  $\lambda$  and  $\lambda'$ , which can be obtained either from experimental results or by computing the stress induced by the presence of one C atom (see detailed procedure in [42]).

The configurational entropy change is defined as (see the [appendix](#)):

$$\begin{aligned} \frac{S(X, Z, T) - S(X, 0, T)}{k_B} = & 2X(1 - Z)\ln[X(1 - Z)] \\ & + X(1 + 2Z)\ln[X(1 + 2Z)] \\ & + 2[1 - X(1 - Z)]\ln[1 - X(1 - Z)] \\ & + [1 - X(1 + 2Z)]\ln[1 - X(1 + 2Z)] \\ & - 3(1 - X)\ln(1 - X) - 3X\ln(X). \end{aligned} \quad (6)$$

Similar expressions of the Gibbs energy can be found in the literature. After the pioneering, but not detailed derivation of Zener [26], Kurdjumov and Khachaturyan [41, 43] and later Zhong [44] proposed a simplified expression of the configurational entropy for dilute systems. Recently, Maugis *et al* [29] derived the same expression for the entropy, but did not provide the detailed calculation of the interaction parameter  $\lambda_0$ .

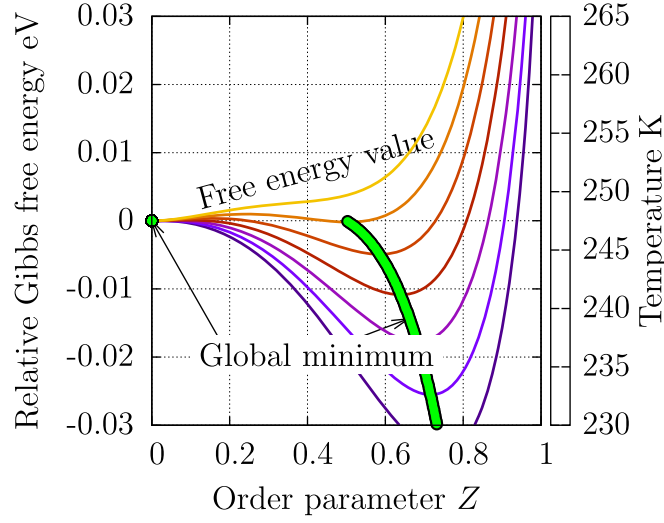


**Figure 3.** Gibbs free energy variation as a function of the order parameter for a carbon content of 2 at%.

The Gibbs energy defined in equation (3) is plotted as a function of the order parameter  $Z$  in figure 3 for different temperatures. Depending on temperature, three cases can be observed: (i) at high temperature ( $T > T^+$ ), the Gibbs energy exhibits only one minimum located at  $Z = 0$ , which corresponds to a fully disordered state. At low temperature ( $T < T^-$ ), only one minimum is observed, but for an order parameter  $Z$  ranging between 0.5 and 1. At intermediate temperatures ( $T^- < T < T^+$ ), two local minima exist: one for  $Z = 0$  and the other one for  $Z = Z_{\min}$ . One of these minima is metastable and the other is stable. The critical temperature  $T_c$  corresponds to the temperature for which the two local minimum have exactly the same energy:

$$G(X, 0, T_c) = G(X, Z_{\min}, T_c). \quad (7)$$

The order parameter  $Z_{\min}$  minimising the Gibbs energy and the critical temperature  $T_c$  can be calculated numerically for all temperatures and concentrations.

Note that  $T_c$  and  $Z_{\min}$  can also be derived from the value of the ordering energy coefficient  $\lambda_0$ , directly calculated from the internal energy of fully ordered  $U(X, 1)$  and fully disordered  $U(X, 0)$  simulation boxes by MS calculations. Instead of using equation (5),  $\lambda_0$  is estimated via (see the [appendix](#))

$$\lambda_0 = \frac{U(X, 1) - U(X, 0)}{3n_{\text{Fe}}X^2}. \quad (8)$$

In the following, we will distinguish between the *mean field* thermodynamic model, where the interaction parameter is calculated from mean-field equation (5) and the *atomistically informed* thermodynamic model, where the interaction parameter is calculated from atomistic simulations.

Finally, strictly speaking, the order/disorder transition is first order (the system has to overpass an energy barrier to go from a metastable state to a stable state), but the energy barrier is so small that the transition will occur almost simultaneously, as if it were a second order transformation.

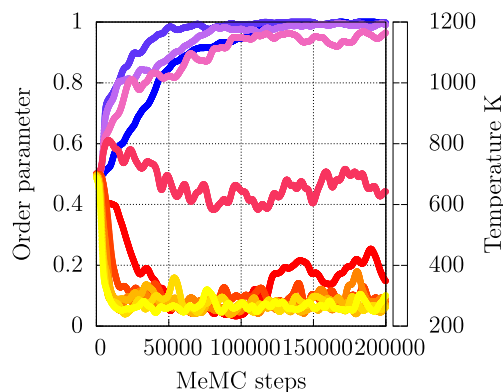


**Figure 4.** Order parameter  $Z$  of MeMC simulation results as a function of the temperature for system containing 9 at%.

## 4. Results

### 4.1. Convergence of MeMC simulations

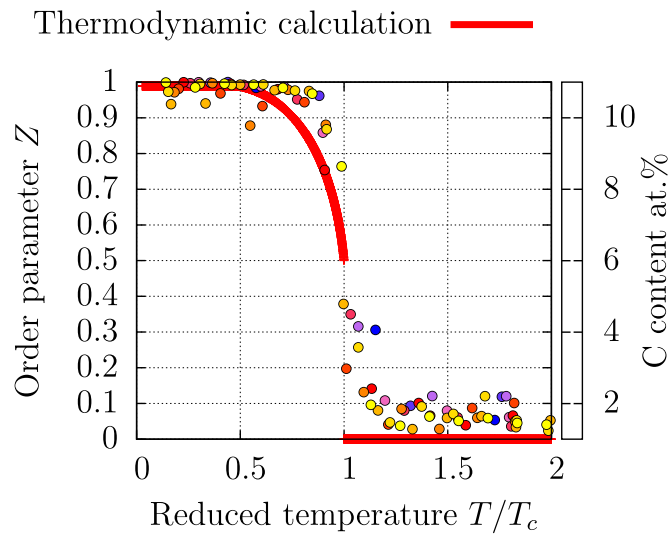
In order to get reproducible results, simulations were launched four times for each set of C concentration and temperature (half ordered-half disordered simulation boxes). The calculation of the order parameter is performed by taking the average value over all simulations. The order parameter  $Z$  of the MeMC simulations over the course of the simulations for 9 at% C are presented in figure 4. From the initial order parameter of  $Z = 1/2$ , most systems converge to either an ordered or a disordered state; the 600 K system seems to remain partly ordered. The measurement of  $Z$  is performed by taking the averages of all results after 100 000 MeMC steps (for which the order parameter is roughly constant).

### 4.2. Order-disorder behaviour given by MeMC and thermodynamic calculation

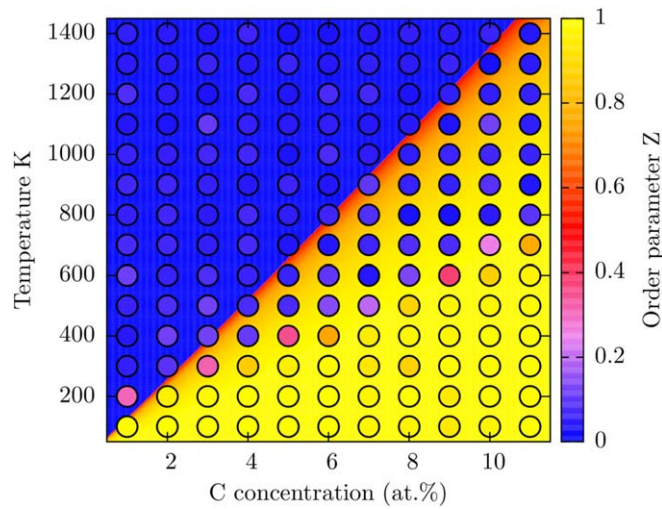
According to the thermodynamic model, the order parameter does not take any value between 0 and 0.5 (see figure 3). In order to determine the critical temperature  $T_c$  from the MeMC simulations, two successive temperatures  $T_1$  and  $T_2$  for which the order parameters fulfil  $Z(T_1) > 0.5 > Z(T_2)$  were considered for each C concentration value. Via a binary search method, new MeMC simulations were launched until  $|T_1 - T_2| = 1$  K (which corresponds to less than ten new simulations per concentration). The transition temperature was then defined as:  $T_c = (T_1 + T_2)/2$ .

Figure 5 shows the order parameter as a function of the reduced temperature  $T/T_c$  for each C concentration for both MeMC and mean field thermodynamic model. For  $T/T_c < 1$ , both approaches exhibit similar results, whereas for  $T/T_c > 1$ , MeMC simulations lead to an order parameter slightly larger than 0 (predicted by thermodynamical model). This may be due to local ordering induced by attractive chemical interactions (see [34]) or finite size effects.

Figure 6 compares the order parameter of MeMC and the mean field thermodynamic model over a wide range of C concentrations and temperatures. A relatively good agreement for lower C concentrations can be seen, although MeMC predicts a somewhat higher transition temperature at 1 at%. At higher C concentrations, the critical temperature predicted by the mean field thermodynamic model is almost twice as high as that of MeMC. In practice,



**Figure 5.** Order parameter as a function of the reduced temperature  $T/T_c$  of the MeMC results and the thermodynamic model.



**Figure 6.** Phase diagram showing the order-disorder transition. Circles: MeMC simulations. Background: mean field thermodynamic model.

these high C concentrations could be expected near defects (i.e. dislocations, grain/lath boundaries) before carbides precipitation. In the following, the origin of this disagreement is investigated.

**4.2.1. Understanding the origin of disagreement between MeMC and mean field thermodynamic model.** The inability of mean field elastic model to accurately predict order-disorder transition temperature has been pointed out by many authors [27, 28, 30, 31]. In our case, two factors may explain the deviation of the MeMC results from the mean field

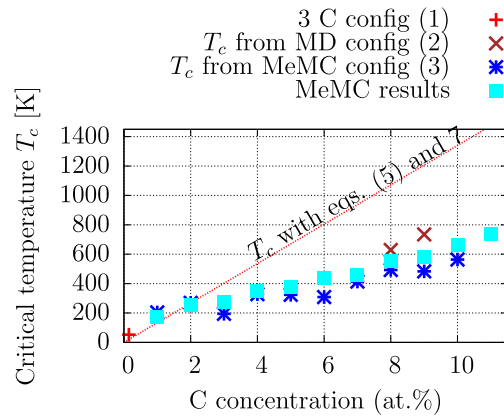


**Figure 7.** Comparison of critical temperature  $T_c$  given by thermodynamical model and MeMC simulations. The thermodynamical model uses the interaction parameter  $\lambda_0$  calculated via mean field approach (equation (5)) or via equation (8) informed by 3C, MD or MeMC configurations.

thermodynamic calculation: (i) Physical quantities such as Young's modulus and/or dipole tensor components, which are considered to be constant in the thermodynamic calculation, may vary with the C concentration. (ii) Local interactions between C atoms may influence Gibbs energy of ordered or disordered states. Concerning the first possibility, Janßen *et al* [45] reported a variation of less than 2% in Young's modulus for the interatomic potential employed in this study for the C concentration of 3 at.%, which is in good agreement with experiments [46]. Therefore, the variation of Young's modulus cannot explain the difference of 800 K for the critical temperature for 11 at.% in figure 7.

To investigate the effect of local atomic configurations on the order–disorder transition temperature, the interaction parameter can be estimated from simulation boxes via calculation of the internal energy of fully ordered and fully disordered simulations boxes (see equation (8)). This way,  $\lambda_0$  accounts for macroscopic elastic energies and also local C–C interactions. Three different configurations were used to evaluate  $\lambda_0$  from simulations:

- (1) Low C limit configurations (3 C): three C atoms are inserted into the simulation box containing only Fe atoms in such a way that C–C interactions can be neglected (C atoms are separated from at least 2.5 nm). For the ordered state, the C atoms are in the same site type. For the disordered state, the C atoms occupy three different site types.
- (2) MD configurations: ordered and disordered states are obtained from MD simulation at 8 at.% and 9 at.% at 900 K and 1400 K (see section 2.2).
- (3) MeMC configurations: fully ordered states are created by inserting the C atoms randomly into  $z$ -sites only, whereas fully disordered states are created inserting the C atoms randomly in  $x$ ,  $y$  and  $z$  sites (see section 2.2).

These three estimations of the interaction parameter can then be straightforwardly re-introduced in equation (5) to get a alternative value of the critical order–disorder transition temperature. Figure 7 compares the critical temperatures obtained from MeMC, mean field and atomistically informed thermodynamic calculation. It can be clearly seen that the atomistically informed thermodynamic model agrees well with MeMC calculations, for the three investigated configurations: (1) low C limit, (2) MD, and (3) MeMC. Accounting for

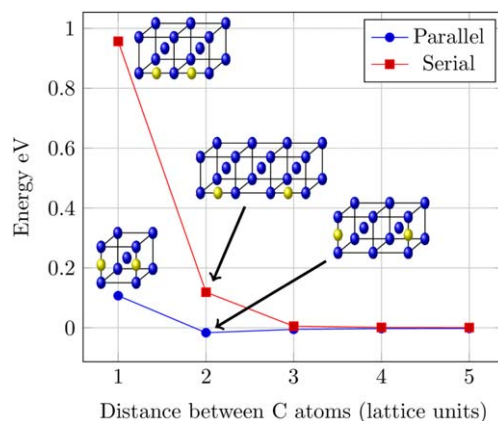


**Figure 8.** Interaction energy values for two C atoms being in the same site type for parallel and serial configurations as a function of the distance between two C atoms.

the mean field elastic energy only, does not provide an accurate estimation of the order-disorder transition temperature; C–C interactions may play a important role.

Concerning the direct C–C interactions, it was previously reported [34], that at short distance the interaction between two C atoms may be repulsive, even if they are in the same site type. In figure 8, it can be seen that the interaction between two C atoms is strongly repulsive, even though they occupy the same type of site (serial ordering). Interaction energy (defined as the energy difference between a box with two interacting C atoms in a given configuration and a box with two infinitely distant C atoms; i.e. a negative interaction energy means attractive interaction) is drastically different when two C atoms do not share the same tetragonal distortion axis (parallel ordering in figure 8), which is energetically much more favorable. This illustrates the importance of including local C–C interactions into account. We recall here that the mean field thermodynamical model does not differentiate between serial and parallel ordering.

Figure 8 shows that C–C configurations, considered by the mean field thermodynamic model as favorable, are, in reality, extremely unfavorable (due to repulsive C–C interactions). In order to account for these unfavorable configurations, serial neighbouring C–C configuration at a distance of one lattice unit could be simply forbidden in the entropic part of the mean field elastic model. If this new assumption is relatively easy to account for in dilute case (one could state that each C atom occupy three site instead of one), the analytical calculation of configurational entropy becomes intractable for concentrated alloys, for which forbidden sites impinge on each other. To overpass this difficulty, the MeMC algorithm can be used to evaluate the improved entropic part of the mean field thermodynamic model. The enthalpy will still be calculated from equation (A.12). In the following, this method will be referred as ‘mean field MeMC’.

It has been checked the mean field MeMC without forbidden site and after convergence, gives exactly the same results as the mean field thermodynamic model.

Figure 9 compares the order parameter  $Z$  of the mean-field MeMC and the transition temperatures of the original mean field thermodynamic model and the MeMC simulations. All three methods give similar results at low C content. However, the mean-field MeMC results deviate strongly from the original mean field thermodynamic model at higher C contents. This proves that forbidding unfavorable high energy configurations strongly impacts the resulting

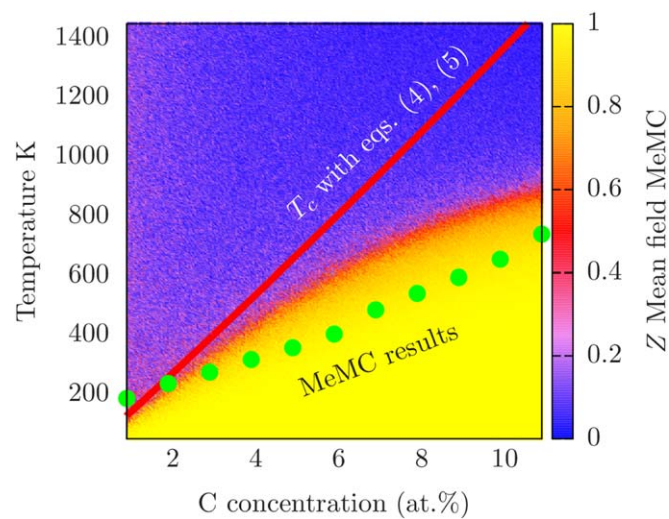


**Figure 9.** Comparison between the order parameter  $Z$  of the mean-field MeMC (background) and the transition temperatures of mean field thermodynamic model and the MeMC simulations (green full circles). Each pixel of the background corresponds to one mean-field MeMC simulation.

order parameter of the mean field thermodynamic model and brings it towards the MeMC simulations. The agreement between MeMC and mean field MeMC is however not perfect since unfavorable configurations are not either strictly forbidden or authorised but rather follow a Boltzmann statistics as described in the MeMC approach.

Therefore, the mean field thermodynamic model, often proposed in the literature, is not valid at high C concentrations, as most of the direct C–C interactions are repulsive and obviously play an important role.

**4.2.2. Local C–C configurations in dilute alloys.** It has been demonstrated that unfavorable C–C configurations need to be accounted for to correctly describe the order–disorder transition of Fe–C systems.

The strongly repulsive C–C configurations have already been discussed but figure 8 also shows attractive configurations (e.g. parallel configuration at two lattice parameters). The mean field thermodynamic calculation does not account for these configurations.

Figure 10 shows the radial distribution function of a 2 at.%C system at 200 and 1000 K, corresponding to ordered and disordered states after MeMC convergence. For the ordered state at 200 K, strong peaks corresponding to the  $\text{Fe}_{16}\text{C}_2$  structure can be seen. This proves that not only is Zener ordering observed, but also full ordering characteristic of the  $\text{Fe}_{16}\text{C}_2$  structure (see [34] or [47]), even for systems with carbon concentrations lower than 11%. These attractive local interactions could explain why, at low carbon content, the critical ordering temperature  $T_c$  is slightly higher than predicted by the mean-field thermodynamic model.

In other words, MeMC simulations exhibit slightly higher critical temperature at low C content, due to local attractive C–C configurations, and much lower critical temperature at high C content due to highly repulsive C–C configurations.

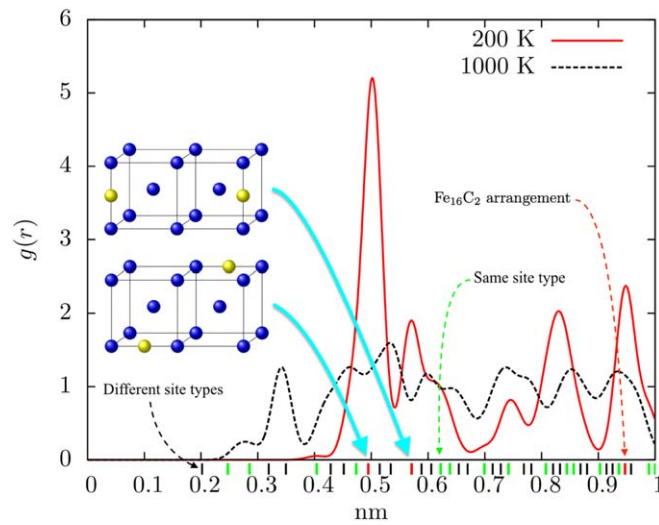


**Figure 10.** Radial distribution function for 2 at.% for the temperatures of 200 and 1000 K. The red lines correspond to the peaks observed in  $\text{Fe}_{16}\text{C}_2$ . Red/green/blue lines under the figure indicate the theoretical distance values of two C atoms of  $\text{Fe}_{16}\text{C}_2$ /ordered/all possible arrangements.

## 5. Conclusion

In this paper, the stability of the Zener ordering of C atoms was studied via atomistic simulations and mean field thermodynamic calculations in a wide range of temperature and C concentrations. The atomistic simulations were performed using a Metropolis Monte Carlo scheme informed by an EAM Fe–C interatomic potential. The mean-field thermodynamic model is based on the estimation of the elastic interaction between C atoms due to tetragonal distortion of octahedral sites.

- Convergence of MeMC simulations is relatively fast, thanks to an optimised simulations procedure.
- Atomistic MeMC simulations strongly disagree with mean-field thermodynamic model, especially at high C concentration. This disagreement due to local strongly repulsive C–C interactions (seen as attractive by the mean-field thermodynamical model).
- If the thermodynamical model is informed by atomistic simulations energies, it then agrees with MeMC simulations.
- Forbidding these local C–C highly energetic configurations in the estimation of the entropy of the system also leads to a better agreement between the thermodynamical model and MeMC.
- At low carbon content, local attractive C–C configurations also slightly modify the energetics of the system, in favour of the ordered configuration.

In conclusion, mean-field thermodynamical model fails to accurately predict the order–disorder transition temperature of Fe–C systems because of local C–C interactions that may strongly modify the hamiltonian of the system.

## Acknowledgments

C Becquart and R Veiga are acknowledged for fruitful discussions on the local minimisation MeMC method. O Waseda gratefully acknowledges the CAPES/COFECUB project 770/13. We are thankful to FLMSN. Simulations were performed on their massively parallel computer P2CHPD. O Waseda and M Perez would like to thank E Clouet and D Rodney for fruitful discussions.

## Appendix. Assessment of the order parameter via free energy calculation

The free energy or Gibbs free energy  $G$  of a system of volume  $V$  containing  $n_C$  C atoms depends on the repartition of C atoms among the octahedral site types. Let us assume a given repartition  $n_C^x$ ,  $n_C^y$  and  $n_C^z$  atoms in site types  $x$ ,  $y$  and  $z$ , respectively. The free energy is given by

$$G = U + pV - TS \quad (\text{A.1})$$

where  $U$  is the energy of the system,  $p$  is the pressure and  $S$  is the entropy. In this study, we consider the stress free case ( $p = 0$ ). In the following, it is assumed that ordering occurs in  $z$ -type sites, i.e. there is the same amount of C atoms in  $x$  and  $y$  octahedral sites, which leads to:

$$n_C = 2n_C^x + n_C^z. \quad (\text{A.2})$$

Hence,  $n_C^z$  is the only free parameter of the system. Consequently, the  $n_C^z$  that gives the minimum free energy is what is looked for. In the following, the energy  $U$  is calculated first, followed by the entropy  $S$ .

It is known that the each C atom induces a macroscopic tetragonal distortion  $\varepsilon_{ij}$  on the lattice, which interacts with the distortion of other C atoms. There are three components that contribute to the total energy  $U$ , the ‘chemical’ contribution  $U_0$ , the elastic stored energy and the interaction energy, such that

$$U = U_0 + \frac{1}{2}VC_{ijkl}\varepsilon_{ij}\varepsilon_{kl} - \sum_{n_C} P_{ij}^{x,y,z}\varepsilon_{ij} \quad (\text{A.3})$$

where  $P_{ij}^{x,y,z}$  is the dipole tensors accounting for the tetragonal distortion of one C atom lying in  $x$ ,  $y$  or  $z$  site type:

$$P_{ij}^x = \begin{bmatrix} \lambda & 0 & 0 \\ 0 & \lambda' & 0 \\ 0 & 0 & \lambda' \end{bmatrix} P_{ij}^y = \begin{bmatrix} \lambda' & 0 & 0 \\ 0 & \lambda & 0 \\ 0 & 0 & \lambda' \end{bmatrix} P_{ij}^z = \begin{bmatrix} \lambda' & 0 & 0 \\ 0 & \lambda' & 0 \\ 0 & 0 & \lambda \end{bmatrix}. \quad (\text{A.4})$$

Since there is no shear induced by the C atoms, both  $P_{ij}^{x,y,z}$  and  $\varepsilon_{ij}$  can be reduced to

$$P_i^x = [\lambda \quad \lambda' \quad \lambda'], \quad \varepsilon_i = \begin{bmatrix} \varepsilon_x \\ \varepsilon_y \\ \varepsilon_z \end{bmatrix}, \quad (\text{A.5})$$

the same for  $P_i^y$  and  $P_i^z$ . The total energy is then

$$U = U_0 + \frac{1}{2}VC_{ij}\varepsilon_i\varepsilon_j - (n_C^x P_i^x + n_C^y P_i^y + n_C^z P_i^z)\varepsilon_i. \quad (\text{A.6})$$

As the total stress  $\sigma_i$  is given by  $\sigma_i = (1/V)(\partial U / \partial \varepsilon_i)$ , on a stress free sample,  $\sigma_i = 0$ , equation (A.6) leads to

$$VC_{ij}\varepsilon_j = (n_C^x P_i^x + n_C^y P_i^y + n_C^z P_i^z). \quad (\text{A.7})$$

Multiplying both sides of this equation by the compliance tensor  $S_{ij}$  leads to the expression of the macroscopic strain tensor induced by a given repartition of C atoms:

$$\varepsilon_i = \frac{1}{V} S_{ij} (n_C^x P_j^x + n_C^y P_j^y + n_C^z P_j^z). \quad (\text{A.8})$$

When shear is not accounted, the compliance tensor  $S_{ij}$  depends on apparent Young's modulus  $E$ , apparent Poisson ratio  $\nu$ , though the contracted expression

$$S_{ij} = \begin{bmatrix} 1/E & -\nu/E & -\nu/E \\ -\nu/E & 1/E & -\nu/E \\ -\nu/E & -\nu/E & 1/E \end{bmatrix}, \quad (\text{A.9})$$

where  $S_{11} = 0.007400 \text{ GPa}^{-1}$  and  $S_{12} = 0.002763 \text{ GPa}^{-1}$ . Replacing equation (A.8) in equation (A.6) leads to

$$\begin{aligned} U &= U_0 - \frac{1}{2} (n_C^x P_i^x + n_C^y P_i^y + n_C^z P_i^z) \cdot \varepsilon_i \\ &= U_0 - \frac{S_{ij}}{2V} \left( \frac{n_C - n_{\tilde{C}}}{2} P_i^x + \frac{n_C - n_{\tilde{C}}}{2} P_i^y + n_{\tilde{C}} P_i^z \right) \\ &\quad \times \left( \frac{n_C - n_{\tilde{C}}}{2} P_j^x + \frac{n_C - n_{\tilde{C}}}{2} P_j^y + n_{\tilde{C}} P_j^z \right) \end{aligned} \quad (\text{A.10})$$

$$= U'_0 + \frac{(1 + \nu)(\lambda' - \lambda)^2}{12VE} (3n_{\tilde{C}} - n_C)^2, \quad (\text{A.11})$$

where  $U'_0$  is independent of  $n_{\tilde{C}}$ . Using the site-fraction  $X = n_C/(3n_{\text{Fe}})$  and the order parameter defined in equation (2)  $Z = (n_{\tilde{C}} - n_C^x)/n_C$ , the energy of the system can be rearranged as

$$U(X, Z) - U(X, 0) = 3n_{\text{Fe}} \lambda_0 X^2 Z^2 \quad (\text{A.12})$$

where  $\lambda_0 = (1 + \nu)(\lambda' - \lambda)^2/(v^{at}E)$  is the interaction parameter. From equation (A.11), the parameter  $\lambda_0$  can also be defined as

$$\lambda_0 = \frac{U(X, 1) - U(X, 0)}{3n_{\text{Fe}} X^2} \quad (\text{A.13})$$

where  $U(X, 1)$  and  $U(X, 0)$  are the internal energy of fully ordered and fully disordered systems, respectively.

Next, the configurational entropy is calculated, which is given by

$$S = k_B \ln \left[ \prod_{i=x,y,z} \frac{n_{\text{Fe}}!}{n_C^i! (n_{\text{Fe}} - n_C^i)!} \right]. \quad (\text{A.14})$$

Stirling's approximation gives

$$\begin{aligned} \frac{S}{k_B} &= 3n_{\text{Fe}} \ln n_{\text{Fe}} - \frac{2n_C(1 - Z)}{3} \ln \left( \frac{n_C}{3} (1 - Z) \right) \\ &\quad - \frac{n_C(1 + 2Z)}{3} \ln \left( \frac{n_C}{3} (1 + 2Z) \right) \\ &\quad - 2 \left( n_{\text{Fe}} - \frac{n_C(1 - Z)}{3} \right) \ln \left( n_{\text{Fe}} - \frac{n_C(1 - Z)}{3} \right) \\ &\quad - \left( n_{\text{Fe}} - \frac{n_C(1 + 2Z)}{3} \right) \ln \left( n_{\text{Fe}} - \frac{n_C(1 + 2Z)}{3} \right). \end{aligned} \quad (\text{A.15})$$

This expression can be rearranged as a function of the carbon site-fraction  $X$  and the order parameter  $Z$ :

$$\begin{aligned}
 -\frac{S(X, Z)}{k_B} = & 2[1 - X(1 - Z)]\ln[1 - X(1 - Z)] \\
 & + 2X(1 - Z)\ln[X(1 - Z)] \\
 & + [1 - X(1 + 2Z)]\ln[1 - X(1 + 2Z)] \\
 & + X(1 + 2Z)\ln[X(1 + 2Z)].
 \end{aligned}
 \tag{A.16}$$

## ORCID iDs

Fabienne Ribeiro  <https://orcid.org/0000-0001-6492-2678>

Michel Perez  <https://orcid.org/0000-0002-7350-4803>

## References

- [1] Roberts-Austen W C 1897 Fourth report to the Alloys Research Committee *Proc. Inst. Mech. Eng.* **52** 31–100
- [2] Jouanny I, Demange V, Ghanbaja J and Bauer-Grosse E 2010 Structural characterization of Fe–C coatings prepared by reactive triode-magnetron sputtering *J. Mater. Res.* **25** 1859–69
- [3] Tau L M and Bennett C O 1986 Reaction of carbon monoxide/hydrogen over an iron/carbon catalyst *J. Phys. Chem.* **90** 4825–32
- [4] Zhang C, Zhou M, Yu X, Ma L and Yu F 2015 Modified iron-carbon as heterogeneous electro-fenton catalyst for organic pollutant degradation in near neutral pH condition: characterization, degradation activity and stability *Electrochim. Acta* **160** 254–62
- [5] Cantergiani E, Fillon A, Lawrence B, Sauvage X, Perez M, Scott C P and Weck A 2016 Tailoring the mechanical properties of steel sheets using FeC films and diffusion annealing *Mater. Sci. Eng. A* **657** 291–8
- [6] Eyre T S and Baxter A 1972 The formation of white layers at rubbing surfaces *Tribology* **5** 256–61
- [7] Moyar G J and Stone D H 1991 An analysis of the thermal contributions to railway wheel shelling *Wear* **144** 117–38
- [8] Lojkowski W, Djahanbakhsh M, Bürkle G, Gierlotka S, Zielinski W and Fecht H-J 2001 Nanostructure formation on the surface of railway tracks *Mater. Sci. Eng. A* **303** 197–208
- [9] Gulino G, Vieira R, Amadou J, Nguyen P, Ledoux M J, Galvagno S, Centi G and Pham-Huu C 2005 C<sub>2</sub>H<sub>6</sub> as an active carbon source for a large scale synthesis of carbon nanotubes by chemical vapour deposition *Appl. Catal. A* **279** 89–97
- [10] Castro C, Pinault M, Coste-Leconte S, Porterat D, Bendjab N, Reynaud C and Mayne-L'Hermite M 2010 Dynamics of catalyst particle formation and multi-walled carbon nanotube growth in aerosol-assisted catalytic chemical vapor deposition *Carbon* **48** 3816
- [11] Weck A, Sinclair C W, Scott C P and Maunders C 2012 Supersaturated  $\alpha$ -iron in vapour-deposited Fe–C thin films *J. Mater. Sci.* **47** 6939–47
- [12] Scott C P, Sinclair C and Weck A 2011 Amorphous Fe<sub>1-x</sub>C<sub>x</sub> coatings as carbon reservoirs for diffusion strengthening of steel sheets *Scr. Mater.* **65** 763–6
- [13] Speigh G R and Leslie W C 1972 Tempering of steel *Metall. Mater. Trans. B* **3** 1043–54
- [14] Allain S, Danoix F, Goune M, Hoummada K and Mangelinck D 2013 Static and dynamical ageing processes at room temperature in a Fe<sub>25</sub>Ni<sub>0.4</sub>C virgin martensite: effect of C redistribution at the nanoscale *Phil. Mag. Lett.* **93** 68–76
- [15] Kalish D and Roberts E M 1971 On the distribution of carbon in martensite *Metall. Mater. Trans. B* **2** 2783–90
- [16] Miller M K, Beaven P A, Brenner S S and Smith G D W 1983 An atom probe study of the aging of iron-nickel-carbon martensite *Metall. Trans. A* **14** 1021–4

- [17] Garcia-Mateo C, Jimenez J A, Yen H-W, Miller M K, Morales-Rivas L, Kuntz M, Ringer S P, Yang J-R and Caballero F G 2015 Low temperature bainitic ferrite: evidence of carbon supersaturation and tetragonality *Acta Mater.* **91** 162–73
- [18] Jang J H, Bhadeshia H K D H and Suh D-W 2013 Solubility of carbon in tetragonal ferrite in equilibrium with austenite *Scr. Mater.* **68** 198
- [19] Xiao L, Fan Z and Jinxiu Z 1995 Lattice-parameter variation with carbon content of martensite. I. X-ray-diffraction experimental study *Phys. Rev. B* **52** 9970
- [20] Bauer-Grosse E 2004 Thermal stability and crystallization studies of amorphous tm-c films *Thin Solid Films* **447-448** 311–5
- [21] Krauss G 1999 Martensite in steel: strength and structure *Mater. Sci. Eng. A* **273-275** 40–57
- [22] Faraoun H I and Zhang Y D 2006 Claude Esling, and Hafid Aourag. Crystalline, electronic, and magnetic structures of  $\theta$ -Fe<sub>3</sub>C,  $\chi$ -Fe<sub>5</sub>C<sub>2</sub>, and  $\eta$ -Fe<sub>2</sub>C from first principle calculation *J. Appl. Phys.* **99** 093508
- [23] Zhang Y, Zhao X, Bozzolo N, He C, Zuo L and Esling C 2005 Low temperature tempering of a medium carbon steel in high magnetic field *ISIJ Int.* **45** 913–7
- [24] Königer A, Hammerl C, Zeitler M and Rauschenbach B 1997 Formation of metastable iron carbide phases after high-fluence carbon ion implantation into iron at low temperatures *Phys. Rev. B* **55** 8143–7
- [25] Kehoe M and Kelly P M 1970 The role of carbon in the strength of ferrous martensite *Scr. Metall.* **4** 473–6
- [26] Zener C 1948 Theory of strain interaction of solute atoms *Phys. Rev.* **74** 639
- [27] Khachaturian A G and Shatalov G A 1955 K teorii uporyadocheniya atomov ugleroda v kristalle martensita *Fiz. Met. Metalloved.* **32** 5
- [28] Udyansky A, Pezold J Von, Bugaev V N, Friák M and Neugebauer J 2009 Interplay between long-range elastic and short-range chemical interactions in Fe-C martensite formation *Phys. Rev. B* **79** 224112
- [29] Maugis P, Danoix F, Zapolsky H, Cazottes S and Gouné M 2017 Temperature hysteresis of the order-disorder transition in carbon-supersaturated alpha-Fe *Phys. Rev. B* **96** 214104
- [30] Naraghi R, Selleby M and Ågren J 2014 Thermodynamics of stable and metastable structures in Fe-C system *Calphad* **46** 148–58
- [31] Chirkov P V, Mirzoev A A and Mirzaev D A 2015 Molecular-dynamics simulations of carbon ordering in BCC Fe and its impact on martensite transition *Mater. Today: Proc.* **2** S553–6
- [32] Lau T T, Först C J, Lin X, Gale J D, Yip S and Van Vliet K J 2007 Many-body potential for point defect clusters in Fe-C alloys *Phys. Rev. Lett.* **98** 215501
- [33] Ruban A V 2014 Self-trapping of carbon atoms in  $\alpha'$ -Fe during the martensitic transformation: a qualitative picture from *ab initio* calculations *Phys. Rev. B* **90** 144106
- [34] Sinclair C W, Perez M, Veiga R G A and Weck A 2010 Molecular dynamics study of the ordering of carbon in highly supersaturated  $\alpha$ -Fe *Phys. Rev. B* **81** 224204
- [35] Becquart C S, Raulot J-M, Bencteux G, Domain C, Perez M, Garruchet S and Nguyen H 2007 Atomistic modeling of an Fe system with a small concentration of C *Comput. Mater. Sci.* **40** 119–29
- [36] Veiga R G A, Becquart C S and Perez M 2014 Comments on ‘atomistic modeling of an Fe system with a small concentration of C’ *Comput. Mater. Sci.* **82** 118–21
- [37] Lawrence B, Sinclair C W and Perez M 2014 Carbon diffusion in supersaturated ferrite: a comparison of mean-field and atomistic predictions *Modelling Simul. Mater. Sci. Eng.* **22** 065003
- [38] Veiga R G A, Perez M, Becquart C S and Domain C 2013 Atomistic modeling of carbon Cottrell atmospheres in bcc iron *J. Phys.: Condens. Matter* **25** 025401
- [39] Veiga R G A, Goldenstein H, Perez M and Becquart C S 2015 Monte Carlo and molecular dynamics simulations of screw dislocation locking by Cottrell atmospheres in low carbon Fe-C alloys *Scr. Mater.* **108** 19–22
- [40] Waseda O, Veiga R G A, Morthomas J, Chantrenne P, Becquart C S, Ribeiro F, Jelea A, Goldenstein H and Perez M 2017 Formation of carbon Cottrell atmospheres and their effect on the stress field around an edge dislocation *Scr. Mater.* **129** 16–9
- [41] Kurdjumov G V and Khachaturyan A G 1972 Phenomena of carbon atom redistribution in martensite *Metallurgical Transactions* **3** 1069–76

- [42] Clouet E, Garruchet S, Nguyen H, Perez M and Becquart C S 2008 Dislocation interaction with C in  $\alpha$ -Fe: a comparison between atomic simulations and elasticity theory *Acta Mater.* **56** 3450–60
- [43] Kurdjumov G V and Khachaturyan A G 1975 Nature of axial ratio anomalies of the martensite lattice and mechanism of diffusionless  $\gamma \rightarrow \alpha$  transformation *Acta Metall.* **23** 1077–88
- [44] Fan Z, Xiao L, Jinxiu Z, Mokuang K and Zhenqi G 1995 Lattice-parameter variation with carbon content of martensite. II. Long-wavelength theory of the cubic-to-tetragonal transition *Phys. Rev. B* **52** 9979
- [45] Janßen J, Gunkelmann N and Urbassek H M 2016 Influence of c concentration on elastic moduli of  $\alpha'$ -Fe<sub>1-x</sub>C<sub>x</sub> alloys *Phil. Mag.* **96** 1448–62
- [46] Gunkelmann N, Ledbetter H and Urbassek H M 2012 Experimental and atomistic study of the elastic properties of  $\alpha'$  Fe-C martensite *Acta Mater.* **60** 4901–7
- [47] Yan J-Y and Ruban A V 2018 Configurational thermodynamics of C in body-centered cubic/tetragonal Fe: a combined computational study *Comput. Mater. Sci.* **147** 293–303